Int. J. Electrochem. Sci., 17 **(2022)** Article Number: 220432, doi: 10.20964/2022.04.22

International Journal of
ELECTROCHEMICAL
SCIENCE
www.electrochemsci.org

Noble-Metal-Free Cu-N/C Supramolecular Catalyst for Highly Efficient Oxygen Reduction Reaction in Neutral Conditions

Huiqian Yang[1], *Min Wang*[2], *Tingting Yang*[1], *Chunxia Li*[1], *Aifeng Li*[1,*], *Jinsheng Zhao*[1,*]

[1] College of Chemistry and Chemical Engineering, Liaocheng University, 252059, Liaocheng, PR. China
[2] School of Medicine, Liaocheng University, Liaocheng, 252059, Liaocheng, PR. China
[*]E-mail: j.s.zhao@163.com (J.S.Zhao); liaifeng@lcu.edu.cn (A.F. Li)

Received: 6 December 2021 / *Accepted:* 28 January 2022 / *Published:* 4 March 2022

This paper mainly uses the molecular recognition principle and synergistic effect to synthesize the functional supramolecular 2,7-bis(4-([2,2':6',2"-terpyridin]-4'-yl)phenyl)-9-(heptadecan-9-yl)-9*H*-carbazole. The nitrogen active sites at both ends of terpyridine are coordinated with metal copper ions to form a metal supramolecular catalyst that contains both the metal and nitrogen active sites. The surface physical structure and elemental analysis of the synthesized complexes were analyzed using SEM and XPS. The redox properties of the catalysts were characterized using chemical characterization methods, such as cyclic voltammetry (CV), linear sweep voltammetry (LSV), and a rotating ring disk electrode (RRDE). The physical and chemical analysis showed that the catalyst was successfully synthesized and that it was subjected to a redox reaction via a four-electron process. Therefore, the prepared metal supramolecular catalyst has good catalytic performance.

Keywords: Noble Metal free; Cu-N/C supramolecular catalyst; Oxygen reduction reaction

1. INTRODUCTION

A fuel cell is a promising renewable and nonexhaustive technology that meets the requirements for clean and efficient energy conversion in fixed and portable equipment[1-2]. It has been one of the focuses of international research in physics, chemistry, and energy science in the past ten years. Recently, fuel cell research has focused on dedicated high-efficiency catalysts and electrode materials[3]. In these catalysts and electrode materials, Pt and its alloys are the most commonly used cathodic catalytic materials in PEMFC systems that are used to catalyze the slow oxidation-reduction reaction to produce the final product water[4,5]. Although the research regarding precious metal catalysts such as Pt/M alloys (M = Fe[6], Co[7,8], Re, Cr[9], Ru[8], and Sn[10]) has made advances, these catalysts are poisonous[11], and their stability and price factors have seriously hampered the practical application of

high-power fuel cells. This is especially problematic for room temperature fuel cells, thus hindering the commercialization of fuel cells[12]. Therefore, the development of new ideas, design of new materials, use of new research methods, and development of a cathode oxygen reduction catalyst that is low cost, has high catalytic activity, and has high stability are the basic development trends of fuel cell research.

In recent years, carbon-supported transition metal nitrogen-containing composites have been considered to be the most promising non-noble metal catalysts that can replace platinum carbon. M/N-doped carbon material coordinates[13], which have excellent oxygen reduction reaction (ORR) electrocatalytic activity, better durability, and environmentally friendly characteristics, hold potential application prospects[13-15]. Metal supramolecular complexes have the advantages of both complex macromolecules and complex polymers and have unique properties that can be combined with a large number of metals and have a variety of coordination points[16-17]. According a supramolecular chemistry study, the molecular recognition and assembly mechanism[18] to construct supramolecular compounds can be used to achieve the purpose of designing new materials that have new structures and special functions [19]. The supramolecular complementary functional groups have strong intermolecular interaction recognition sites and exhibit strong reactivity and activity in the construction of supramolecular organic crystals. A characteristic nitrogen-containing heterocyclic compounds is that the N atom contains a plurality of isolated electrons, and therefore, it is susceptible to metal ion coordination. Metal organic supramolecular complexes can form a series of special structures[20], such as linear and mesh, and thus, it shows good host and guest performance[21].

For nearly a period of time, with imidazole and phthalocyanine ring of large molecular matrix formed functional supramolecular materials by molecular recognition and self-assembly has been one of the focuses of international research in chemistry and materials science. Organic ligands that contain a bipyridine structure have been studied extensively because of they have a diversity of multiple coordination centers and structures. Because of the introduction of metal ions, metal supramolecular polymers related to conventional supermolecules have a special nature in terms of photoelectrons[22], oxygen reduction[23], and catalysis. Geng et al. compared three-dimensional and sheet-like porphyrin supramolecular compounds and demonstrated that photogenerated electrons improve the performance of a catalyst[24]. Brown et al. reported a cationic ruthenium half-sandwich complex encapsulated in an aqueous supramolecular body[16]. Metal terpyridine supramolecular catalysts are an important topic in the field of supramolecular catalysis. In 2002, Schubert adopted a monomer with a triadopyridine group at the ends, a hydrophilic diethylene glycol spacer unit in the middle, and metal coordination via divalent iron ions in solution. Water-soluble metal supramolecular polymers have been formed via self-assembly[25]. In 2005, Würthner coordinated a small molecule that contained bistopyridine groups to metal zinc ions; the molar ratio of metal zinc ions to the host molecules was controlled appropriately to obtain a larger molecular weight and fluorescent supramolecular polymers[26]. This metal-supramolecular complex retains the guest function of metal organic molecules and protects the complexes from being dissolved. This new metal supramolecular catalyst was formed via self-assembly, and self-design is theoretically feasible; it can be used in room temperature fuel cells and promotes the commercialization of fuel cells. To ensure that a battery has high-energy conversion efficiency, the catalyst is usually highly dispersed in carbon black. To achieve a fuel cell cathode for high catalytic efficiency for ORR, the key steps are to use molecular precursors that contain nitrogen and to use the

above active sites to coordinate with metal ions, forming M-N at active sites of the metal supramolecular catalyst.

In this study, we successfully synthesized the metallo-supramolecular polymer (Cu-BTPHC/C) by employing the bidentate ligand (BTPHC) as a nitrogen-riched precursor. Copper-supramolecular polymers are easily formed via the complexation of copper ions with BTPHC, which has two coordination sites (tripyridine structures) at both ends. When coordinated with copper ions, tripyridine molecules form a coordination polymer (Cu-BTPHC) that consists of alternating chains of ligand and iron. It is known that tripyridine is one of the most effective ligands because of its high binding affinity to metal ions. The synthesis procedure are shown in Scheme 1. To increase the electrochemical performance of the catalyst, we loaded the catalyst onto carbon black as a support in order to enhance the conductivity and stability of the catalyst. We used a series of electrochemical tests and physical characterization techniques to investigate the electrocatalytic performance and the relationship between the catalysts. X-ray diffraction (XRD) and scanning electron microscopy (SEM) were used to evaluate the surface microstructure and the composition of chemical elements. From the test data of the rotating ring electrode, we propose the reaction kinetics and a mechanism of oxygen reduction. Both electrochemical measurements and stability for ORR were tested in 0.1 mol of phosphate buffer solution (PBS) solution. The catalyst has good redox properties due to various test results closing to platinum.

2. EXPERIMENTAL

2.1 Materials

2,7-Bis(4-([2,2':6',2"-terpyridin]-4'-yl)phenyl)-9-(heptadecan-9-yl)-9*H*-carbazole(BTPHC) were synthesized according to a procedure reported in a previous work. The procedure and the experiments for synthesizing that catalysts are described in detail in Scheme 1. 4'-(4-bromophenyl)-3,2':6',3"-terpyridine (BTP), 2,2'-(9,9-dioctyl-9H-fluorene-2,7-diyl)bis(1,3,2-dioxaborinane) (DFB), dimethylformamide (DMF), $PdCl_2(PPh_3)_2$, $Cu(ClO_4)_2 \cdot 6H_2O$, K_2CO_3, $NaH_2PO_4 \cdot 2H_2O$, $K_3[Fe(CN)_6]$, $Na_2HPO_4 \cdot 12H_2O$, acetonitrile (ACN), and isopropanol (99.5 %) were all analytical grade and were purchased from Aladdin Co., Ltd. Nafion (5 wt% in ethanol) and carbon (Vulcan XC-72) were obtained from Nanjing Hui Yu Energy Technology Co., Ltd. Pure nitrogen and oxygen were used to prepare the corresponding saturated electrolyte.

2.2 Synthesis of BTPHC[27]

In a 100 mL round-bottom flask, 489.1 mg (0.7 mmol) of BTP and 543.6 mg (1.4 mmol) of DFB, 25 mL of DMF and 5 mL of 2 M K_2CO_3 were added. The solution in the flask was degassed and recharged with N_2 for three time, and after that, 40 mg of $Pd[P(C_6H_5)_3]_4$ was added to the flask under the protection nitrogen atomosphere. The flask was equipped with a condenser, and the solution in it was bathed in the N_2 atmosphere with the the help a balloon. The flask was placed in a oil bath and be heated to reflux with constant magnetic stirring, and the reaction lasted for 48 hours. After the mixture was

cooled down to room temperature, the target product was extract with chloroform and rinsed with water for three times. And then, the organic phase was dried with anhydrous magnesium sulfate, and filtrate was obtained by filtration. The solvent was distilled away by vaccum distillation. The raw product was purified with column chromatography with a mixture solution of dichloromethane/n-hexane as the eluent. The resultant product BTPHC was obtained as white powder with a yield of 65%.

The ^{1}H NMR (400 MHz, cdcl$_3$) and ^{13}C NMR (101 MHz, cdcl$_3$) data are shown in Fig.1. ^{1}H NMR (400 MHz, CDCl$_3$): δ, 8.86 (s, 4H), 8.81-8.86 (m, 8 H), 8.21 (dt, J=16.8, 8.4 Hz, 2H), 8.07 (t, J=12.0 Hz, 4H), 7.90 (td, J=7.8, 1.7 Hz, 8H), 7.74-7.53 (m, 4H), 7.37 (ddd, J=16.7, 8.3, 5.9 Hz, 4H), 2.51-2.37 (m, 1H), 2.11-1.99 (m, 1H), 1.4-1.09 (m, 24H), 0.93-0.76 (m, 8H).

^{13}C NMR (101 MHz, CDCl$_3$): δ 156.24 (s), 155.94 (s), 149.10 (s), 143.01 (s), 136.89 (d, J=13.2 Hz), 128.05 (s), 127.69 (s), 121.34 (s),118.64 (s), 77.30 (s), 76.99 (s), 76.67 (s), 33.81 (s), 31.72 (s), 29.85-29.06 (m), 26.84 (s), 22.56 (s), 14.03 (s).

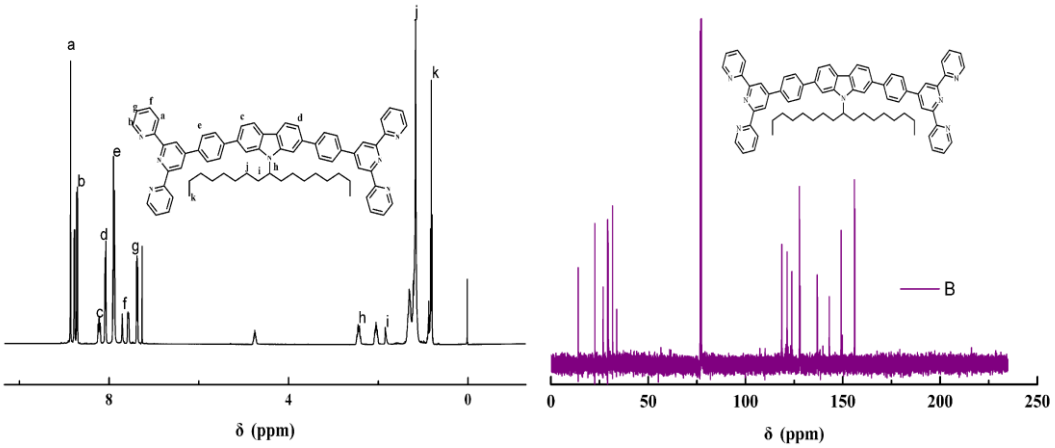

Figure 1. ^{1}H NMR and ^{13}C NMR of BTPHC

2.3 Synthesis of Cu-BTPHC

The ligand BTPHC (26.14 mg, 0.026 mmol) was dissolved in 5 mL of CH_3CN under an atmosphere of nitrogen. Then, $Cu(ClO_4)_2{\cdot}6H_2O$ (9.7 mg, 0.026 mmol) was dissolved in 5 mL of CH_3CN, and the solution was added dropwise to the ligand solution within 30 min under the protection of nitrogen gas. The final mixed solution was then subjected to continuous ultrasonic vibration for 30 min. Finally, the mixture was stirred and refluxed at 90 °C for 1 h under nitrogen atmosphere, as a resultant, a yellow colored solution as the catalyst was obtained, and be labelled as Cu-BTPHC, and this was the target product.

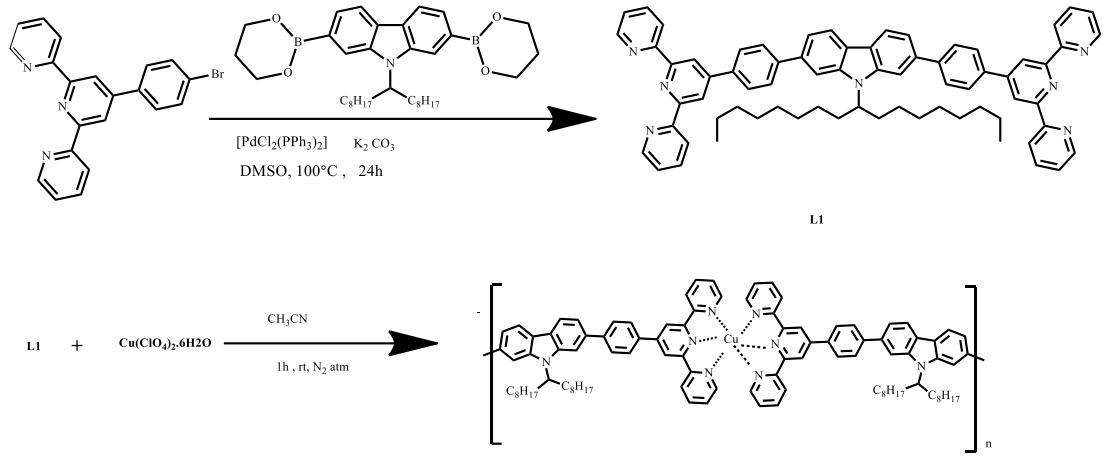

Scheme 1. Synthesis route of Cu-BTPHC polymer

2.4 Preparation of the catalyst-modified electrode

To obtain high performance for the modified electrode, The following methods was used to prepare the catalyst suspension: 1.6 mg of Vulcan XC-72 was dispersed in a mixed solvent consisting of 177 μL of isopropanol, 7 μL of Nafion, and 570 μL of Cu-BTPHC catalyst solution, and then the homogeneous catalyst suspension was obtained after continuous ultrasonic oscillation for 30 min. To obtain the catalyst film, 8.5 μL of catalyst suspension was added dropwise onto the surface of the glass carbon (GC) electrode. The amount of the catalyst was 0.062 mg·cm^{-2}, and catalyst film was then dried in a room atmosphere. For comparison purpose, the commercial Pt/C catalyst (20% Pt content) was also used for the test. For this, the slurry was prepared as follows: 1 mg of Pt/C, 177 μL of isopropanol, 3.5 μL of Nafion solution, and 570 μL of ultrapure water was added to a 1.5 mL centrifuge tube. And the mixture was subjected to ultrasonic oscillation for 30 min. The homogeneous solution (11 μL) was dropped onto the surface the glass electrode (Pt =151 μg cm^{-2}) and then dried at room temperature. The catalyst modified GC electrodes were used as the working electrode in the electrochemical measurements. Before the modification of the electrode, it was polished with Al_2O_3 to get the mirror surface, and then distilled water was used to clean the electrode.

2.5. Physical characterization

^{1}H NMR spectra were measured on an NMR spectrometer (Bruker DPX-400). Scanning electron microscopy (SEM, SU8020) was used to measure the microstructure of Cu-BTPHC. SEM images were recorded on a Merlin Compact (Zeiss) at 15 kV (EHT=15 KV, WD=8.3 nm). The main application of XPS is to determine the electron binding energy, which indicates the qualitative analysis of the surface elements that include the valence state. The electron binding energy from XPS was referenced to C 1s of contamination at 284.5 eV.

2.6. Electrochemical characterization

To obtain a better understanding of the electrochemical properties of the catalyst, we conducted cyclic voltammetry (CV), linear sweep voltammetry (LSV), and rotating ring disk electrode (RRDE) measurements on computer-controlled Autolab potentiostat/galvanostat (PGSTAT302N) and a standard three-electrode electrochemical system. The saturated calomel electrode (SCE) and platinum electrode were used as the reference electrode and counter electrode, respectively. We usually used a PBS solution (0.1 mol pH=7) as a bath solution. All procedures were conducted under a room atmosphere.

3. RESULTS AND DISCUSSION

3.1 Surface morphology of Cu-BTPHC/C catalyst

To study the catalytic activity of the catalyst on a fuel cell, it is necessary to know the surface morphology and elemental composition of the catalyst. Fig. 2 shows the microscopic morphology of pure carbon and Cu-BTPHC/C, as observed using SEM with a magnification of 10,0000 times. As seen from Fig. 2a, the particles of Vulcan X-72 have a spherical shape, and the radius of the spherical particles was about 35-60 nm, and the particles were arranged irregularly to form pore structure (piled pore). As seen in Fig. 2b, the morphology of Cu-BTPHC/C was obviously different from that of the Vulcan X-72 carbon. The rougher surface of the as prepared catalyst indicates that the the Cu-BTPHC/C catalyst was coated on the surface of the carbon powder. The radius of the Cu-BTPHC/C catalyst was obviously larger than that of pure carbon, which shows irregular clusters. The increase in the pore size of the catalyst would enhance the contact area between oxygen and the catalyst and provides a large number of transport channels for the electrolyte.

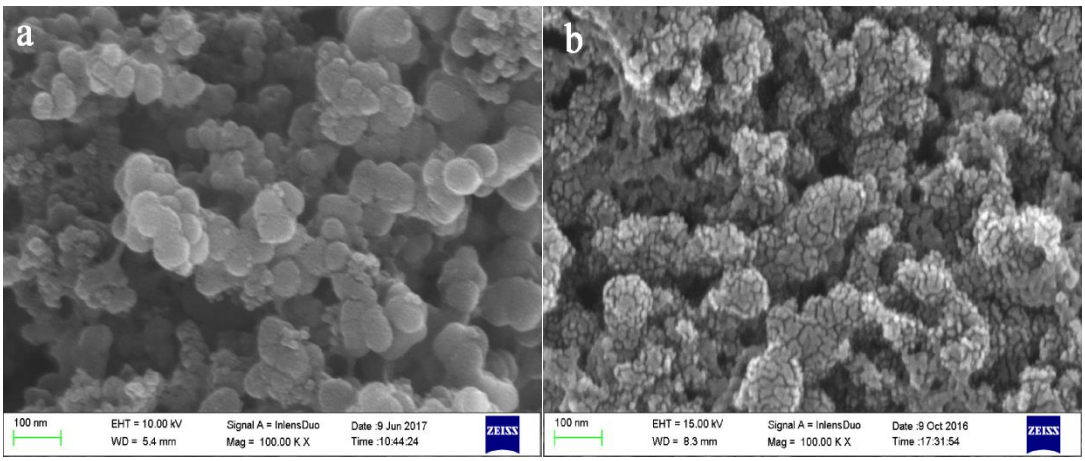

Figure 2. SEM images of (a) C and (b) Cu-BTPHC/C.

3.2. XPS analysis of the structure of the catalyst surface

In this study, X-ray photoelectron spectroscopy was used to characterize the elemental composition of the catalyst. From the survey scan of Cu-BTPHC/C, it is seen that the catalyst contains four kinds of elements: carbon (71.82%), nitrogen (7.15%), oxygen (5.25%), and copper (0.58%). This observation is consistent with the structure and composition of the composite catalyst. The N 1s spectrum can be divided into two peaks at 400.704 eV and 400.101 eV, as shown in Fig. 3a. A peak at a binding energy (BE) of 400.704 eV is attributed to the peak of pyrrolic nitrogen, which is consistent with the presence of the carbazole unit within the polymer. The other most abundant peak was at a binding energy of 400.101 eV and is assigned to the pyridinic peak, which is originated from the existence of the bidentate tripyridine unit along the backbone of the polymer. The position of the pyridinic-N is more positive than it is in most of the previous reports, and this indicates the formation of the complex between the pyridinic nitrogen and copper ion [28-29]. Also, pyridinic N can serve as metal-coordination sites because of its lone-pair electrons. There is a high content of this kind of ORR active nitrogen in our Cu-BTPHC/C catalyst, and this would lead to high catalytic activity.

To further demonstrate that the metal copper ions are coordinated to the polymer, we show the XPS spectrum of the copper element. As seen in Fig. 3b, two pairs of split peaks are clearly observed in the spectrum, and these can be assigned to the binding energies of the Cu $2p_{3/2}$ and Cu $2p_{1/2}$ characteristic peaks, respectively. The peaks at 935.696 eV (Cu $2p_{3/2}$) and 956.096 eV (Cu $2p_{1/2}$) are corresponding to the dissociative copper ions, whereas the peaks of copper in the complex state are located at 936.192 eV (Cu $2p_{3/2}$) and 955.368 eV (Cu $2p_{1/2}$). The movement of copper peaks indicates that copper ions were successfully coordinated to the polymer. In addition, there are two peaks at 936.192 eV and 964.007 eV that may correspond to the copper oxide formed via the oxidation of copper ions during the reaction process. From the above analysis of the XPS spectra of the catalysts, we successfully determined that the synthesis was successful, and the structural characteristics of the complex catalyst Cu-BTPHC/C were characterized.

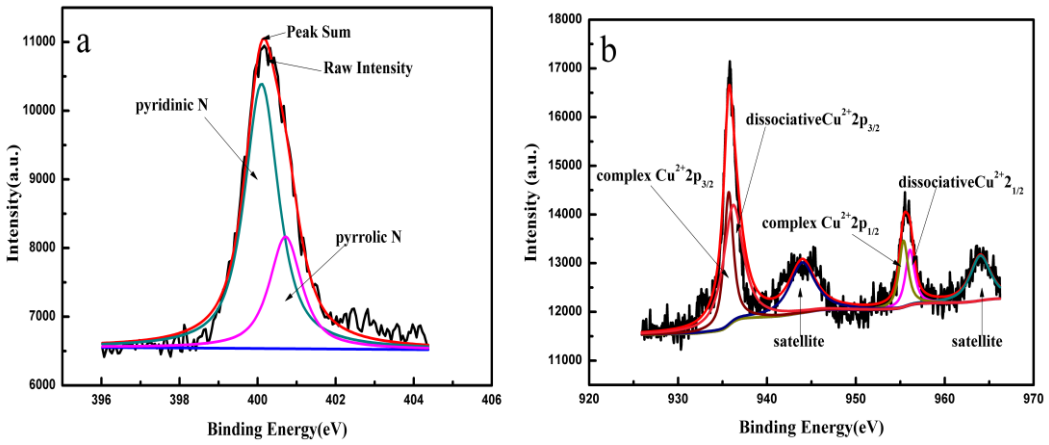

Figure 3. XPS spectra of (a) N 1_S and (b) Cu 2p for Cu-BTPHC/C.

3.3 Electrochemical activity of the Cu-BTPHC/C catalyst toward ORR

On the basis of the electrochemical properties, an aqueous solution of the catalyst complex was prepared and adsorbed onto the surface of the platinum electrode. First, CV was used to study the electrochemical performance of the catalysts in PBS (0.1 M) solution in both saturated N_2 and O_2, respectively. The voltage range of the cyclic voltammograms was from -0.19 V to 1.1 V, and the scan rate was 100 mV /s.

As seen in Fig. 4a, when the electrode was in an environment of saturated N_2, the CV curve had an oxidation peak at 0.58 V, the reduction peak at 0.39 V was less obvious, and the corresponding current amplitude was -0.11 mA. The pair of redox peaks is attributed to the redox potential Cu^{+}/Cu^{2+}. As seen from the curve, the redox reaction is irreversible. In contrast, when the electrode was placed in an environment of saturated O_2, there was a sharp and high reduction peak at 0.37 V, and the corresponding current amplitude was -0.58 mA, there is an increase of 0.47 mA in current amplitude compared to that of the electrode in N_2 atmosphere. The increase in the reduction current value can be attributed to the cathodic oxygen reduction process. The results show that the catalyst exhibited obvious redox activity in the O_2 environment.

To objectively evaluate the electrochemical properties of the catalysts, the CV of the as-prepared catalyst was compared with that of the commercial Pt/C catalyst. The CV of Pt/C catalyst was recorded in an O_2-saturated PBS solution. The test voltage range was from 0.01 V to 1.21 V (vs. RHE), and the scan rate was 100 mV/s. The result is shown in Fig. 4b. By comparison, the initial reduction voltage of the Cu-BTPHC/C was more negative than that of the Pt/C electrode, but the current of the former catalyst was three times larger than that of commercial Pt/C catalyst. Thus, we can conclude that although the nature of the Cu-BTPHC/C catalyst is not as good as that of Pt/C, but the higher reduction current can still give the catalyst good electrochemical properties.

To evaluate the properties of the Cu-BTPHC/C catalyst, cycling durability tests were carried out for 500 CV cycles in the potential of ranging from -0.19 V to 1.11 V (vs. RHE) with a scan rate of 100 mV/s. As seen in Fig. 4c, the maximum current density of the catalyst reduction peak did not show a significant decline after the 500th cycle compared to that of the 1st cycle, and this indicates that the catalyst has good electrochemical stability. At the same time, the maximum current density of Cu-PBTPP/C decreased by 3.17% after 500 cycles of running.

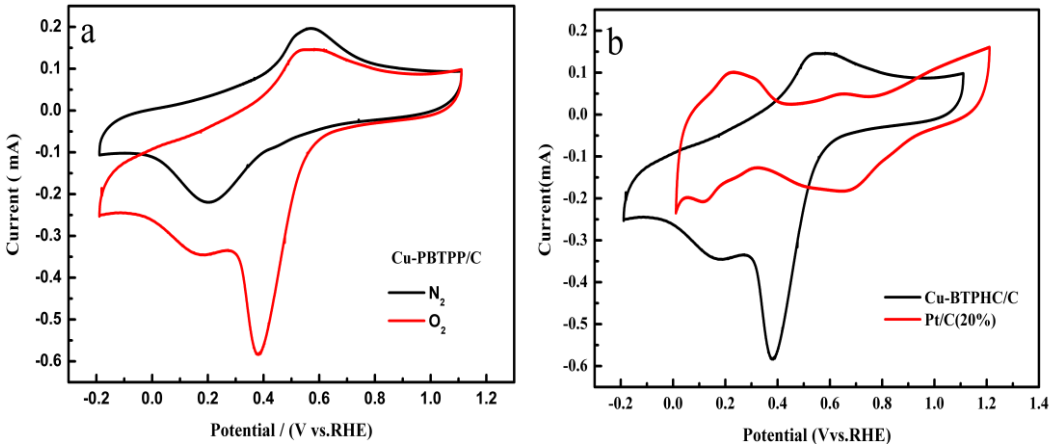

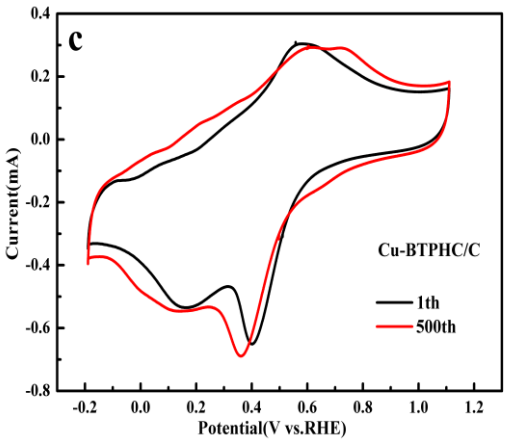

Figure 4. (a) CV of Cu-BTPHC/C in PBS saturated with N_2 and O_2, (b) CV of Cu-BTPHC/C and Pt/C in PBS saturated and O_2, (c) CV of Cu-BTPHC/C in PBS O_2-saturated PBS. Scan rate:100 mV/s.

For a more comprehensive understanding of the redox properties of the catalyst, the linear CV curves of Cu-BTPHC/C were recorded at different rotation rates from 400 to 1600 rpm to determine the ORR activity of Cu-BTPHC/C in 0.1 mol PBS solution. And the voltage range was set from 0.81 to -0.19 V. Generally, it is believed that a $4e^-$ process is more efficient than a $2e^-$ process, since the former process generate H_2O and the latter process generate H_2O_2, and H_2O_2 is poisonous to the activity of the catalyst. The ORR polarization curves of Cu-BTPHC/C are shown in Fig. 5a. As clearly seen in the graph, the polarization curves of the catalyst at different speed linear scanning curves are similar. In addition, every polarization curve has the same initial reduction potential, and the corresponding current densities increased with the increase in the rotation speed. This demonstrates that more and more oxygen passes through the electrode surface and participates in the ORR process when the rotation speed is increased. There are two distinct areas in the polarization curves that were measured in O_2-saturated PBS solution. One is the mixed kinetic control region (0.1-0.6V) where the current is mainly affected by the rate of charge transfer reaction and the rate of mass transfer. The other is the diffusion control region (potential less than 0.1 V), where the current reaches a maximum and is only controlled by the mass transfer rate. The initial reduction potential for oxygen of Cu-BTPHC/C is 0.6 V, and the limiting current is 0.41 mA. In the LSV of Cu-BTPHC/C, an obvious ORR activity is observed. Nevertheless, only the LSV curves cannot fully characterize the catalytic activity of the catalyst, and thus, we compared the results of the ORR activity of 20 wt % Pt/C from 0 V to 1.2 V vs RHE in PBS (0.1 mol). The test results are shown in Fig. 5b and 5c. It was found that the polarization curve of Cu-BTPHC/C and Pt/C have the similar shape. The differences are that the onset reduction potential and the limiting current of the Pt/C catalyst were 0.9 V and 5 mA, respectively. Both the onset reduction potential and the current amplitude of the catalyst are a little inferior to that of the Pt/C catalyst.

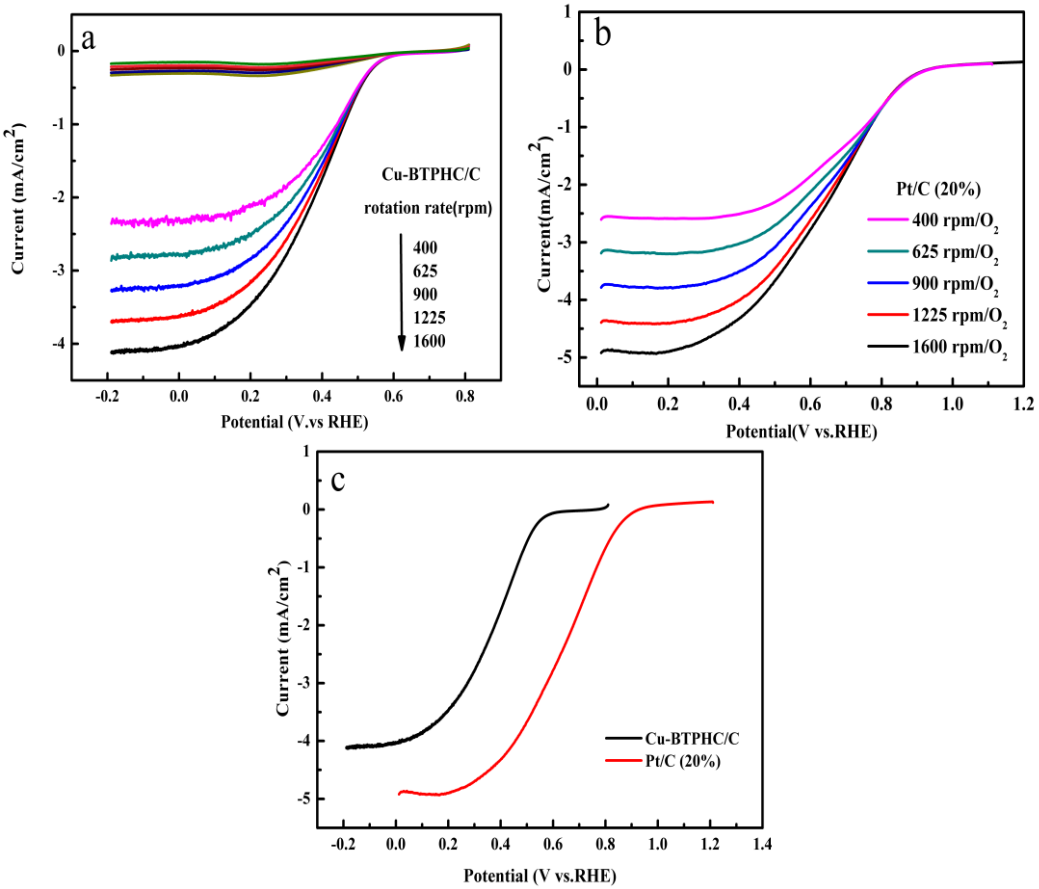

Figure 5. (a) Polarization curves of Cu-BTPHC/C at various rotating rates in PBS solution saturated with O_2 and N_2. (b) Polarization curves of Pt/C at various rotating rates in PBS solution saturated with O_2. (c) Polarization curves of Cu-BTPHC/C and Pt/C at the rotating rate of 1600 rpm.

The number of electrons transferred in the ORR-modified disk electrode was calculated using the Koutechy-Levich equation (1-2)[30,31], which was established using the data obtained from RDE measurements.

$$\frac{1}{i} = \frac{1}{i_k} + \frac{1}{Bw^{1/2}} \qquad (1)$$

Here, i is the measured disk current destiny, i_k is the kinetic current destiny, *w* is the rotation speed of the RDE electrode (w = 2πN and N is the rotation speed), and B is the Koutechy-Levich slope given by Equation 2.

$$B = 0.62nFcD^{2/3}v^{-1/6} \qquad (2)$$

Table 1. The parameters and their values

n	The number of electrons transferred	
F	Faraday's constant	96485 C mol^{-1}

c	The concentration of oxygen (pH=7-13)	$C_{O_2}=1.2\times10^{-3}molL^{-1}$
v	kinematic viscosity of the electrolyte	$1.00\times10^{-2}cm^2s^{-1}$
D	diffusion coefficient of oxygen (pH=7)	$D=1.9\times10^{-5}\mathrm{cm}^2s^{-1}$

Table 1 listed the parameters and their values, and to calculate the value of n, the plots of $1/i$ versus $w^{-1/2}$ for different rotation rates in the Koutechy-Levich region were obtained using the Koutechy-Levich equation. These plots are shown in Fig. 6a, which shows that the curve has a similar tendency to that of the the Pt/C catalyst (Fig. 6b). There is a good linear relationship between $1/i$ and $w^{-1/2}$. By substituting the slope values into Equation 2, the corresponding transfer numbers are calculated to be 3.9 (-0.11 V), 3.9 (0.01 V), 3.8 (0.11 V) and 3.7 (0.21 V), respectively. These values indicate that the catalyst followed a nearly four-electron-transfer pathway, and this corresponds to the complete reduction of oxygen to water.

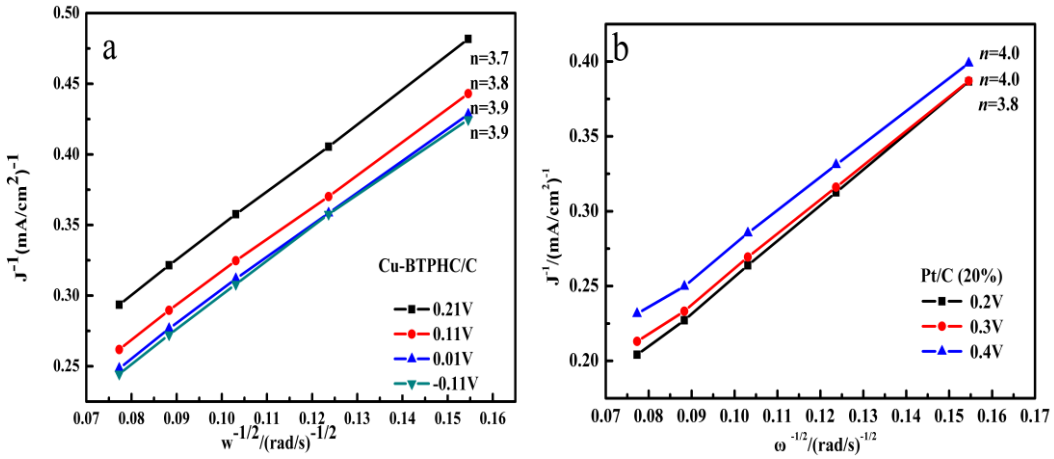

Figure 6. K-L plots at the potential values of 0.21 V, 0.11 V, 0.01 V, and -0.11 V for (a) Cu-BTPHC/C and (b) at the potential values of 0.2 V, 0.3 V, and 0.4 V for Pt/C.

RRDE is commonly used for detecting intermediate products and for studying the electrode reaction. Hydrogen peroxide is generated in the process of oxygen reduction reaction. Thus, we can calculate the amount of the produced H_2O_2 to determine if the process is a 4 electron transfer process. Due to the more close to the number of 4 electrons of the oxygen reduction, the less amount of H_2O_2 was discharged. Meanwhile, H_2O_2 has a great influence on the corrosion of fuel cells, and hence, the 4 electron process is more desirable than the 2 electron process.

The average number of electron was 3.8 obtained from the RDE test, and thus, the ORR reaction on the Cu-BTPHC/C catalyst is more inclined to occur via the four-electron transfer process. To prove this, we measured the RRDE curve of the catalyst at different rotating rates in 0.1 M PBS to determine the production yields of H_2O_2 in the ORR process. To ensure that all of the H_2O_2 can be oxidized and detected, the ring potential was set at 0.6 V(vs. Ag/AgCl), and the disk potential ranged from -0.19 V to 0.8 V(vs. RHE) for Cu-BTPHC/C. The ORR curves of the catalysts were recorded from 400 to 1600

rpm at a scan rate of 10 mV/s, and the results are shown in Fig.7a (for Cu-BTPHC/C) and Fig.7b (Pt/C). The upper part is the ring current, and the lower part is the disk current. The disk current increased with an increase in the speed, and this corresponds to decreased ring current. To precisely confirm the overall electron number for the catalyzed ORR, the percentage of H_2O_2 was detected quantitatively using the RRDE technique during the oxygen reduction process. We can determined the number of electrons number (n) and the value of $\%H_2O_2$ yielded using the following equations[32]:

$$n = \frac{4-(I_r/I_d)}{N} \quad (3)$$

$$\%H_2O_2 = \frac{(I_r/I_d)}{N} \times 100 \quad (4)$$

Here, N is the RRDE collection efficiency of H_2O_2, which was determined to be 0.37 in this study. I_r and I_d are the currents at the ring and disk electrodes, respectively. As seen in Fig. 7e, the average n value obtained from the Koutecky-Levich plot is 3.87, which is close to the value from RRDE analysis, and this indicates that the date is reliable. As seen in Fig. 7c, the $\%H_2O_2$ production decreased continuously with an increase in the rotation rates, and the maximum output of H_2O_2 was not higher than 7.56%. This is because the high-speed rotation during the test causes the intermediate product that is produced on the disk electrode to diffuse rapidly onto the ring electrode. Table 2 listed the electrocatalytic performance of some supramolecular-based non-noble catalysts for ORR reported in recent years, the data show that the catalyst reported in the present study is comparable to the state of the art catalysts reported recently.

The trends observed in Fig.7a and 7c indicate the ORR mechanism is strongly potential-dependent. We also measured the RRDE of the Pt/C electrode (Fig.7b) and obtained the n value and the H_2O_2yield of the catalyst; the RRDE curve for these measurements are shown in Fig.7(e) and Fig.7(f).

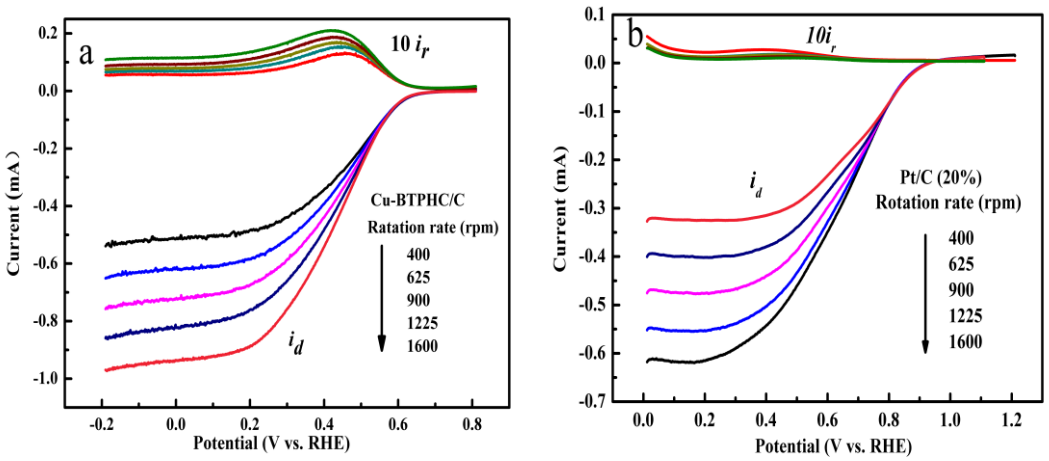

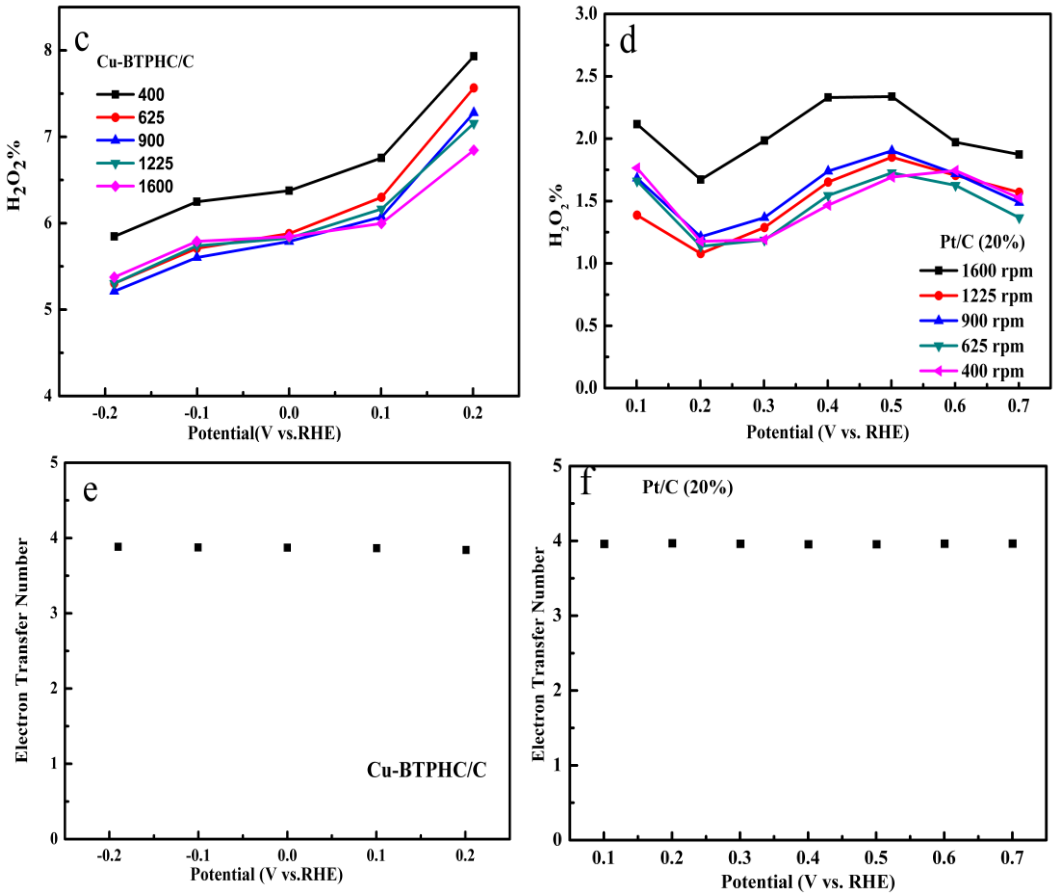

Figure 7. RRDE curves of Cu-BTPHC/C(a), Pt/C (b), the hydrogen peroxide yields of Cu-BTPHC/C (c) and Pt/C(d), (e) ETN of Cu-BTPHC/C, and (f) ETN of Pt/C.

Table 2. Electrocatalytic performance of some supramolecular-based non-noble catalysts for ORR reported in recent years.

Catalyst	E_{onset} (V)	$E_{1/2}$ (V)	ENT	Average H_2O_2(%)	Electrolyste solution	Reference electrode	Ref.
Cu-BTPHC/C	0.67	0.43	3.87	6.63%	PBS(pH=7)	RHE	This study
Pt/C (20%)	0.90	0.63	4.0	1.6%	PBS(pH=7)	RHE	This study
PMPhen-Cu/C	0.61	0.35	3.95	3.0%	PBS(pH=7)	RHE	17
Cu-SOCBP/C	0.62	0.44	3.8	9%	PBS(pH=7)	RHE	13
CuPPyPhen/C	0.62	-	4.0	7.8%	PBS(pH=7)	RHE	38
Cu-CTF/CPS	0.81	-	3.85	-	PBS(pH=7)	NHE	37
Cu-HT/Au	0.74	-	3.7	-	Britton-Robinson buffer(pH=7)	NHE	39

The ORR data obtained via RRDE is mainly used for semi-quantitative analysis of oxygen reduction of a catalyst[13]. For the ORR-catalyzed pathway on the platinum electrode in PBS solution, the type of ORR that occurs on the electrode can be divided into two steps. A large number of oxygen

molecules can firstly obtain two electrons and are reduced to H_2O_2 and then be further reduced to water. The reaction producing H_2O_2 is often referred to as the two-electron reaction pathway. Another major pathway is a reaction process in which it does not appear to be possible to detect H_2O_2. That is, oxygen molecules directly undergo four-electron reduction to H_2O or OH^-, and this is often known as the four-electron reaction pathway. The mechanism is demonstrated in Equations (5-7)[33,34], and the corresponding reaction rates for each step are denoted as k_1, k_2, and k_3, respectively.

$$O_2 + 4H^+ + 4e^- \xrightarrow{k_1} 2H_2O \quad (5)$$

$$O_2 + 2H^+ + 2e^- \xrightarrow{k_2} H_2O_2 \quad (6)$$

$$H_2O_2 + 2H^+ + 2e^- \xrightarrow{k_3} 2H_2O \quad (7)$$

The rate constants k_1, k_2, and k_3 can be calculated according the following equations:[35-36]

$$k_1 = S_2 Z_{O_2} \frac{I_1 N - 1}{I_1 N + 1} \quad (8)$$

$$k_2 = \frac{2 Z_{O_2} S_2}{I_1 N + 1} \quad (9)$$

$$k_3 = \frac{Z_{H_2O_2} N S_1}{I_1 N + 1} \quad (10)$$

where $Z_{O_2} = 0.62 D_{O_2}^{2/3} v^{-1/6}$ and $Z_{H_2O_2} = 0.62 D_{H_2O_2}^{2/3} v^{-1/6}$ ($D_{H_2O_2}$ and D_{O_2} are diffusion coefficients of H_2O_2 and O_2, respectively, in PBS solution.). I_1 and S_1 are respectively the intercept and slope from plots of I_d/I_r vs. $w^{-1/2}$. S_2 is the slope from the plot of $I_d/(I_{dl} - I_d)$ vs. $w^{-1/2}$ plot. (I_{dl} is the disk-limiting current).

The values of k_1, k_2 and k_3 are shown in Fig. 9a. From the data, we can conclude that $k_1 \gg k_2 \approx k_3$ at the potential. k_1 is much bigger than k_2, and k_2 is slightly larger than k_3. This suggests that oxygen may be reduced to H_2O at a faster rate with a subsequent reduction of O_2 to H_2O_2 at a slower rate. These results prove that there is a small amount of H_2O_2 present. Therefore, the ORR catalyzed by Cu-BTPHC/C should be via the coexistence of a directed and two step four-electron reaction. In addition, Fig. 9b shows the ratio of rate constants (k_1/k_2) of the Cu-BTPHC/C catalyst as a function of electrode potential. The ratio of k_1/k_2 keep a unity, which varied around 15 at the potential rage of -0.2 to 0.2 V. Ultimately, this result may indicate that the direct four-electron transfer process is the dominant reaction pathway.

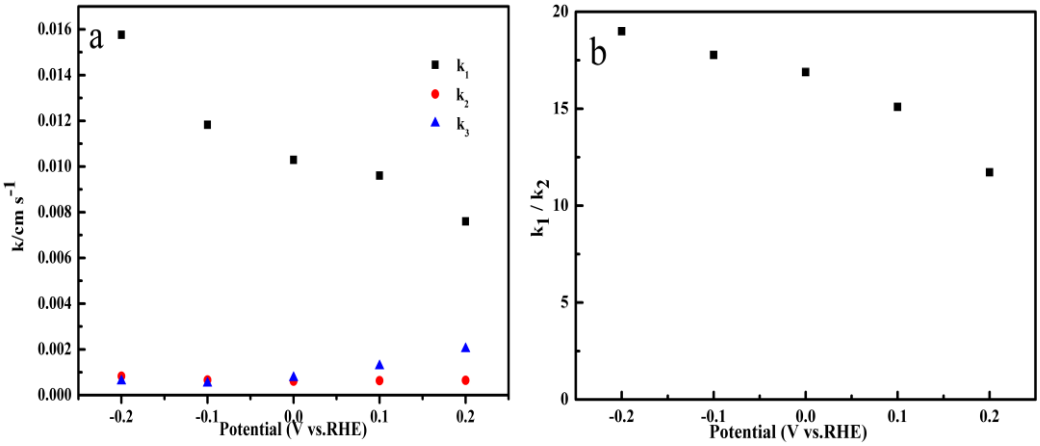

Figure 9. (a) k_1, k_2, and k_3 of the ORR pathway model for Cu-BTPHC/C, (b) the ratios of k_1/k_2.

4. CONCLUSIONS

In this paper, a bidentate ligand containg two tripyridine as the coordination sites are synthesized. The ligand has a strong coordination effect and is coordinated with metal ions to form a new metal supramolecular catalyst. Each of the supramolecules contains two pyridine rings at both ends, and copper ions connect via nitrogen atoms on the adjacent pyridine rings. The copper ions form a six-coordinate structure, and the adjacent molecules connect to form linear molecules. The physical and electrochemical characterization of this catalyst demonstrated that the catalyst was primarily converted to water at the cathode via a four-electron process. However, as seen from the data, the starting potential and current of the catalyst cannot achieve the effect of the commercial Pt/C catalyst, and thus, further research is needed.

References

1. P. Kavanagh, *Curr. Opi. Electrochem*., 29 (2021) 100765.
2. T. Li, Y. Yang, X.X. Wang, K.Q. Zheng, S.L. Shen, X.M. Ou, B. Lin, P.Z. Feng, S.R. Wang and Y.H. Ling, *J. Power. Sources*., 512 (2021) 230533.
3. T. Huang, J.H. Wei, X.T. Zhu and E. Zhang, *Int. J. Hydrogen. Energ*., 46 (2021) 30334.
4. M. Torihata, M. Nakamura, N. Todoroki, T. Wadayama and N. Hoshi, *Electrochem. Commun*., 125 (2021) 107007.
5. L.Y. Gong, J. Liu, Li Yang, X. Wang, E. Luo, J. Zhao, J.J. Ge, C.P. Liu and W. Xing, *Chem. Eng. J*., 428 (2022) 131569.
6. Z.H. Yan, M. Wang, J.F. Liu, R.M. Liu and J.S. Zhao, *Electrochim. Acta*, 141 (2014) 331.
7. G. Shi, H. Yano, D.A. Tryk, A. Liyama and H. Uchida, *ACS Catal.*, 7 (2017) 267.
8. G. Sievers, S. Mueller, A. Quade, F. Steffen, S. Jakubith, A. Kruth and V. Brueser, *J. Power Sources.*, 268 (2014) 255.
9. M.K. Jeon and P.J. McGinn, Co-alloying effect of Co and Cr with Pt for oxygen electro-reduction reaction. *Electrochim. Acta.*, 64 (2012) 147.
10. C.T. Hsieh, Y.S. Chang and K.M. Yin, *J. Phys. Chem. C.*, 117 (2013) 15478.

11. N.S. Nasri, J.M. Jones, V.A. Dupont and A. Williams, *Energy Fuel*, 12 (1998) 1130.
12. D. Singh, K. Mamtani, C.R. Bruening, J.T. Miller and U.S. Ozkan, *ACS Catal*, 4 (2014) 3454.
13. Y.Y. Zhao, Y. Chu, X.P. Ju, J.S. Zhao, L.Q. Kong and Y. Zhang, *Catalysts*, 8 (2018) 53.
14. M.Yang, Y.J. Liu, H.B. Chen, D.G. Yang and H.M. Li, *ACS Appl. Mater. Interfaces.*, 8 (2016) 28615.
15. M.N. Banis, S. Sun, X.B. Meng, Y. Zhang, Z.Wang, R.Y. Li, M. Cai, T.K. Sham and X.L. Sun, *J. Phys. Chem. C*., 117 (2013) 15457.
16. C.J. Brown, G.M. Miller, M.W. Johnson, R.G. Bergman and K.N. Raymond, *J. Am. Chem. Soc.*, 133 (2011) 11964.
17. Y. Chu, L. Gu, X.P. Ju, H.M. Du, J.S. Zhao and K.G Qu. *Catalysts.*, 8 (2018) 245.
18. X.Y. Hu, T.X. Xiao, C. Lin, F. Huang and L.Y. Wang, *Acc. Chem. Res.*, 47 (2014) 2041.
19. Y. Peng, H. Zhang, H. Wu, B. Huang, L. Gan and Z. Chen, *Dyes Pigments.*, 87 (2010) 10.
20. H.Y. He, M. Wang, J.S. Zhao, Y. Zhang. *Chem Eng J.*, 316 (2017) 680.
21. N.C. Gianneschi, P.A. Bertin, S.T. Nguyen, C.A. Mirkin, L.N. Zakharov and A.L. Rheingold, *J. Am. Chem. Soc.*, 125 (2003) 10508.
22. G. Schwarz, I. Haßlauer and D.G. Kurth, From terpyridine-based assemblies to metallo-supramolecular polyelectrolytes (MEPEs). *Adv. Colloid Interface Sci.*, 207 (2014) 107.
23. J.Q. Tian, R. Ning, Q. Liu, A.M. Asiri, A.O. AI-Youbi and X.P. Sun, *ACS App. Mater. Interfaces.*, 6 (2014) 1101.
24. G. Geng, P. Chen, B. Guan, L. Jiang, Z. Xu, D. Di, Z. Tu, W. Hao, Y. Yi and Chen C. *ACS Nano*, 11(2017) 4866.
25. S. Schmatloch, M.F. González, U.S. Schubert, *Macromol. Rapid. Comm.*, 23 (2002) 957.
26. R. Dobrawa, M. Lysetska, P. Ballester, M. Grüne and F. Würthner, *Macromolecules*, 38 (2005) 1315.
27. M.D. Hossain, T. Sato, M. Higuchi, *Chem-Asian J.*, 8 (2013) 76.
28. J.M.L. Martínez, E. Rodríguez-Castellón, R.M.T. Sánchez, L.R. Denaday, G.Y. Buldain and V.C. Dall'Orto, *J. Mol. Catal. A- Chem.*, 339 (2011) 43.
29. F.F. Wang, P.J. Wei, G.Q. Yu, J.G. Liu, *Chem- Eur. J.*, 22 (2016) 382.
30. N.S. Parimi, Y. Umasankar, P. Atanassov and R.P. Ramasamy, *ACS Catalysis*., 2 (2012) 38.
31. L. Lin, Q. Zhu and A.W. Xu, *J. Am. Chem. Soc.*, 136 (2014) 11027.
32. W. Niu, L. Li, X. Liu, N. Wang, J. Liu, W. Zhou, Z. Tang and S. Chen, *J. Am. Chem. Soc.*, 137 (2015) 5555.
33. Y. Chu, H.M. Du, K.Q. Qu, Y. Zhang, J.S. Zhao and Y. Xie, *Int. J. Hydrogen. Energ.*, 43 (2018) 21810.
34. G. Panomsuwan, N. Saito and T. Ishizaki, *Carbon*, 98 (2016) 411.
35. N.S.Parimi, Y. Umasankar, P. Atanassov, R.P. Ramasamy, *ACS. Catalysis.*, 2 (2011) 38.
36. L. Gu, Y.Y. Dong, H.M. Du, Y. Zhang, Q. Yuan, B. Wang, H.M. Wang, J.S. Zhao and N.Q. Zhang, *Catal Surv. Asia.*, 24 (2020) 219.
37. K. Iwase, T. Yoshioka, S. Nakanishi, K. Hashimoto, K. Kamiya, *Angew. Chem. Int. Ed.,* 54(2015)11068.
38. Y.Q. Lu, X.L. Wang, M. Wang, L.Q. Kong, J.S. Zhao, *Electrochim. Acta.*, 180(2015) 86.
39. M. Kato, N. Oyaizu, K. Shimazu, I. Yagi. *J. Phys. Chem.*, 120(2016)15814.